ICSV14
Cairns • Australia
9-12 July, 2007

14th International Congress on Sound & Vibration

APPLICATION OF RATIONAL ORTHOGONAL WAVELETS TO ACTIVE SONAR DETECTION OF HIGH VELOCITY TARGETS

David Bartel[1 *], Limin Yu[2 †], Lang White[2 ‡]

[1]Maritime Operations Division
Defence Science and Technology Organisation
Australia 5111

[2]School of Electrical and Electronic Engineering
The University of Adelaide
Australia 5005

[*]david.bartel@dsto.defence.gov.au
[†]limin.yu@eleceng.adelaide.edu.au
[‡]lang.white@eleceng.adelaide.edu.au

Abstract

This paper is concerned with the problem of detecting moving targets using active sonar. We study a promising class of waveform, the Rational Orthogonal Wavelets (ROWs), designed to be tolerant of multipath Doppler spreading. Recent work in communication has shown that ROWs are effective even on severely spread channels. We apply ROWs for the first time to target detection. ROW pulses are compared to conventional CW and LFM pulses via simulations involving a high–speed target in shallow water. The target is point–like, and ray tracing is used to synthesize Doppler–shifted multipath arrivals in a range–independent environment. The key feature of ROWs that we exploit is the orthogonality they maintain over a wide range of delays and Doppler scales. Thus the maximum–likelihood detector is a simple average of matched filters, and the statistics of the detector under the null hypothesis are known, permitting CFAR operation. In addition, a fast algorithm resulting in rational scaled filter banks is available.

1. INTRODUCTION

The fourth–generation (4G) cellular communication system is the next major mobile phone standard [1]. 4G is predicted to deliver rich multimedia content at a nominal rate of 100 Mbps in outdoor environments, providing users with features such as mobile TV [2]. Multipath interference and Doppler spreading are significant problems to be addressed by 4G system designers, as users receive broadband content at highway speeds and in urban areas. In recent work a new class of signalling waveform, the Rational Orthogonal Wavelet (ROW), showed promise in mitigating severe multipath Doppler spreading by adding an extra dimension of diversity, this being the set of dominant eigenrays in the multipath channel [3]. This paper explores the use of ROWs in the detection of targets in shallow water, a problem that also suffers from multipath Doppler.

The remainder of this paper is organised as follows. In section 2 we introduce the ROWs and give some of their properties. Section 3 describes the time series simulations. Section 4 describes the results, giving Receiver Operating Characteristic (ROC) data to compare the ROW pulses against conventional CW and LFM pulses.

2. RATIONAL ORTHOGONAL WAVELETS

A Complex Rational Orthogonal Wavelet (CROW) is a complex function $\psi_+(t) = \psi(t) + i\hat{\psi}(t)$, where $\psi(t)$ is a Real Rational Orthogonal Wavelet (RROW) and $\hat{\psi}(t)$ is the Hilbert transform of $\psi(t)$ [3, 4]. $\psi(t)$ and $\hat{\psi}(t)$ are real functions of time t, and $\psi_+(t)$ is thus an analytic signal, with frequency spectrum

$$\Psi_+(\omega) = \begin{cases} 2\Psi(\omega), & \omega > 0 \\ \Psi(0), & \omega = 0 \\ 0, & \omega < 0, \end{cases} \tag{1}$$

where $\Psi(\omega)$ is the frequency spectrum of $\psi(t)$, given by

$$\Psi(\omega) = \begin{cases} (2\pi)^{-\frac{1}{2}} \exp\left(i\frac{\omega}{2}\right) \sin\left(\frac{\pi}{2}\beta\left(q\left(\frac{|\omega|-\omega_1}{\omega_1}\right)\right)\right), & \omega_1 \le |\omega| < \omega_2 \\ (2\pi)^{-\frac{1}{2}} \exp\left(i\frac{\omega}{2}\right) \cos\left(\frac{\pi}{2}\beta\left(q\left(\frac{|\omega|-\omega_2}{\omega_2}\right)\right)\right), & \omega_2 \le |\omega| \le \omega_3 \\ 0, & |\omega| \notin [\omega_1, \omega_3]. \end{cases} \tag{2}$$

The definition (2) provides a family of RROWs, $\{\psi_q(t)\}$ say, indexed by $q \in \{1, 2, ...\}$. Function $\beta(x) = x^4(35 - 84x + 70x^2 - 20x^3)$ is used to ensure $\psi(t)$ decays smoothly and rapidly away from $t = 0$ [3]. The angular frequency markers ω_1, ω_2 and ω_3 in (2) are given by

$$\omega_1 = 2q^2(2q+1)^{-1}\pi, \tag{3}$$
$$\omega_2 = a\omega_1 = 2q(q+1)(2q+1)^{-1}\pi, \quad \text{and} \tag{4}$$
$$\omega_3 = a\omega_2 = 2(q+1)^2(2q+1)^{-1}\pi, \tag{5}$$

where $a = 1 + (1/q)$ is a rational dilation factor. Since $\omega_3 - \omega_1 = 2\pi$, $\Psi(\omega)$ has support on $\{\omega : -\omega_3 \le \omega \le -\omega_1\} \cup \{\omega : \omega_1 \le \omega \le \omega_3\}$, and $\psi(t)$ therefore has support over all $t \in \mathbb{R}$. In practice, however, the construction function $\beta(x)$ ensures that $\psi(t)$ decays rapidly for large $|t|$, and $\psi(t)$ is effectively limited to $t \in [-8, 8]$.

Figure 1 displays the first four RROWs and their frequency spectra, where each wavelet is normalized to have maximum amplitude unity. Note that $\Psi(\omega)$ has Hermitian symmetry ($\Psi(-\omega) = \Psi^*(\omega)$) so that we need only display and work with the positive portion of the spectral support, $\{\omega : \omega_1 \le \omega \le \omega_3\}$.

Consider the collection of complex functions

$$\psi_{+,kl}(t) = \frac{a^{k/2}}{\sqrt{2}}\psi_+\left(a^k t - lq\right), \qquad k, l \in \mathbb{Z}. \tag{6}$$

These functions are scaled and delayed replicas of the CROW $\psi_+(t)$, and $\{\psi_{+,kl}(t)\}$ forms an

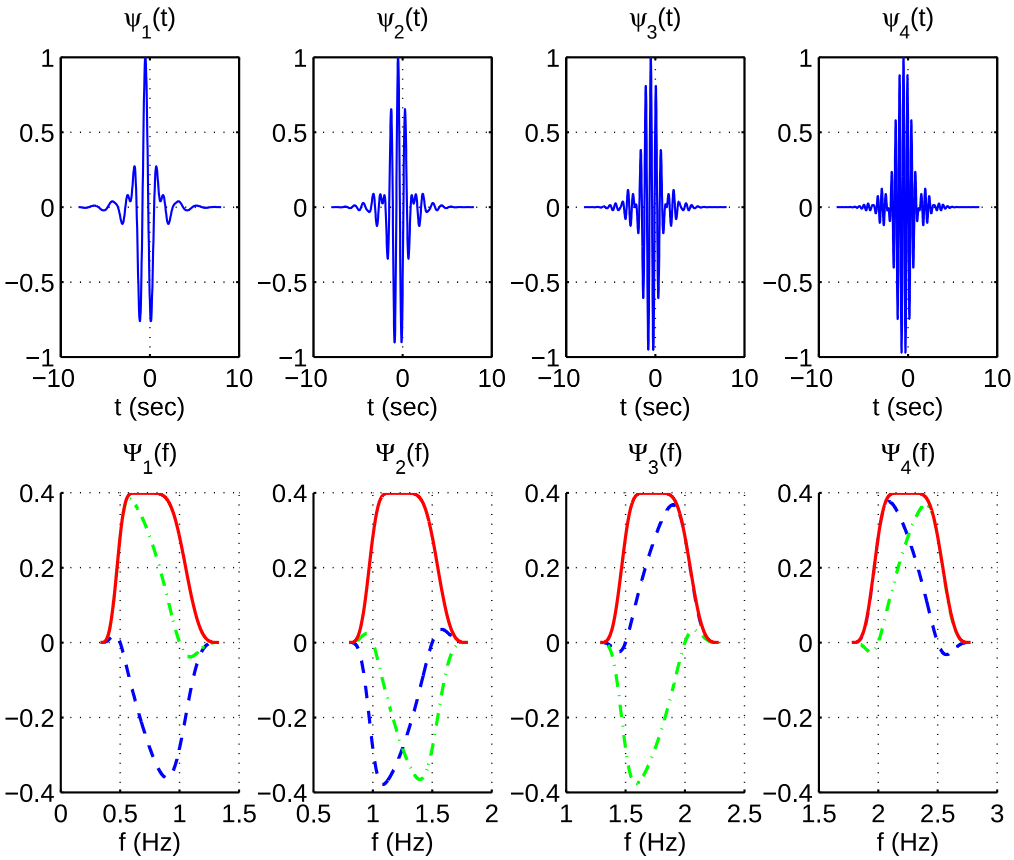

Figure 1. Time series and frequency spectra of the first four RROWs. The upper figures show the time series, normalized to unit amplitude and over $t \in [-8, 8]$; the lower figures give the matching spectra, over just the positive–frequency portions of the spectral support. The dashed (blue) curves are the real parts $\Re\left(\Psi_q(f)\right)$; the dash–dotted (green) curves are the imaginary parts $\Im\left(\Psi_q(f)\right)$; and the solid (red) curves are the magnitudes $|\Psi_q(f)| = \sqrt{\left(\Re\left(\Psi_q(f)\right)\right)^2 + \left(\Im\left(\Psi_q(f)\right)\right)^2}$, for $q \in \{1, 2, 3, 4\}$.

orthonormal basis of the complex–valued Hilbert space $L^2\left(\mathbb{R}\right)$, with orthonormality defined by

$$\int \psi_{+,kl}(t)\psi^*_{+,mn}(t)dt = \delta_{km}\delta_{ln}, \quad k, l, m, n \in \mathbb{Z}. \tag{7}$$

It is this orthogonality property that is explored in the current work on the detection of fast–moving targets in shallow water, where we investigate whether multipath returns can be separated in delay–scale space and combined to obtain a processing gain over conventional CW and LFM pulses. We will use CROWs as signals, and compare their detection performance against CW and LFM pulses.

3. SIMULATION MODEL

The ocean–acoustic environment used in our simulations is a fluid–over–solid extension of the Pekeris model [5]. A uniform water layer of thickness $h = 100\,\mathrm{m}$, density $\rho_1 = 1000\,\mathrm{kg}\cdot\mathrm{m}^{-3}$ and speed of sound $c_1 = 1500\,\mathrm{m}\cdot\mathrm{s}^{-1}$ is bounded above by a pressure–release surface and below by a uniform solid half–space. Frequency–dependent sound absorption $\alpha_1(f)$ dB$\cdot\lambda_1^{-1}$ in seawater is modelled with the Francois–Garrison equation, where $\lambda_1 = \frac{c_1}{f}$ is the wavelength of sound in water at source frequency f Hz [6]. The bottom halfspace has uniform density $\rho_2 = 2000\,\mathrm{kg{\cdot}m^{-3}}$, compressional (P–wave) speed $c_{2\mathrm{P}} = 1800\,\mathrm{m{\cdot}s^{-1}}$, shear (S–wave) speed $c_{2\mathrm{S}} = 600\,\mathrm{m{\cdot}s^{-1}}$, and attenuation coefficients $\alpha_{2\mathrm{P}} = 0.7\,\mathrm{dB}{\cdot}\lambda_{2\mathrm{P}}^{-1}$ and $\alpha_{2\mathrm{S}} = 1.5\,\mathrm{dB}{\cdot}\lambda_{2\mathrm{S}}^{-1}$, where $\lambda_{2\mathrm{P}} = \frac{c_{2\mathrm{P}}}{f}$ and $\lambda_{2\mathrm{S}} = \frac{c_{2\mathrm{S}}}{f}$ are the wavelengths of P– and S–waves, respectively, at source frequency f Hz. These parameters were chosen to approximate a "coarse sand" basement [7].

A transceiver and target, both point–like, moved within the water, each at a fixed speed, heading and depth. The transceiver moved at depth $z_s = 25\,\mathrm{m}$ below the ocean surface, and at constant speed $v_s = 30\,\mathrm{m{\cdot}s^{-1}}$ along the line $x = v_s t$, $y = 0$, $z = z_s$ (due East). The target moved at depth $z_t = 5\,\mathrm{m}$ and at constant speed $v_t = 30\,\mathrm{m{\cdot}s^{-1}}$ along the line $x = 6000 - v_t t$, $y = 0$, $z = z_t$ (due West). The closest point of approach of target and transceiver was at simulation time $t = 100\,\mathrm{s}$, with the target directly above the transceiver.

Geometrical acoustics (classical ray tracing) was used to synthesize the echo time series produced when the target was ensonified with a given pulse [8]. Note that the material absorption coefficients $\alpha_1(f)$, $\alpha_{2\mathrm{P}}$ and $\alpha_{2\mathrm{S}}$ were treated in the formula for the planewave bottom reflection coefficient by allowing the speeds c_1, $c_{2\mathrm{P}}$ and $c_{2\mathrm{S}}$ to be complex:

$$c_1 \leftarrow c_1 \left(1 + i\alpha_1(f)\eta^{-1}\right)^{-1}, \tag{8}$$

$$c_{2\mathrm{P}} \leftarrow c_{2\mathrm{P}} \left(1 + i\alpha_{2\mathrm{P}}\eta^{-1}\right)^{-1}, \quad \text{and} \tag{9}$$

$$c_{2\mathrm{S}} \leftarrow c_{2\mathrm{S}} \left(1 + i\alpha_{2\mathrm{S}}\eta^{-1}\right)^{-1}, \tag{10}$$

where $i^2 = -1$ and $\eta = 40\pi \log_{10} e$ is a conversion factor required when attenuation coefficients are specified in decibels per wavelength.

Data for three different pulses was generated from separate simulation runs. Each pulse had a time duration of $T = 1/2\,\mathrm{s}$ and was transmitted over the absolute time interval $0 \le t \le T$. Approximately 1.02 s of coherent time series data was synthesized at the transceiver at output rate $F_s = 131\,072\,\mathrm{Hz}$, over sample numbers $k \in \{1007865, \ldots, 1142162\}$, where sample k was synthesized at absolute time $t = kT_s$ for $k \in \{1, 2, \ldots\}$, with $T_s = 1/F_s$ being the time between samples. This data begins at the earliest time kT_s at or after the first arrival of the echo at the transceiver, and ends after a drop in dynamic range in the received time series of about 30 dB.

The three transmit waveforms used in this study were a Continuous Wave (CW) pulse, of frequency 25 kHz; a Linear Frequency Modulation, Upsweep (LFMU) pulse, of centre frequency 25 kHz and bandwidth 1 kHz; and a CROW pulse, with wavelet index $q = 1562$. The CROW was defined in section 2 as having a temporal support of 16 s. In the simulations, each pulse was transmitted over the interval $0 \le t \le 1/2$, so the CROW pulse was compressed in time by a factor of 32. Hence the transmitted CROW pulse had positive–frequency spectral support over the 32 Hz–wide band $32f_1 \le f \le 32f_3$ where $32f_1 = 32q^2/(2q+1) \approx 24\,984\,\mathrm{Hz}$ and $32f_3 = 32(q+1)^2/(2q+1) \approx 25\,016\,\mathrm{Hz}$. Figure 2 shows the time–frequency support of the transmitted CROW pulse. Note the good localisation in both time and frequency.

4. DETECTION PERFORMANCE

Using the simulation model discussed above, noise–free time series data $\{y_1(k)\}$, $\{y_2(k)\}$ and $\{y_3(k)\}$ were generated for the three separate pulses, where $k \in \{1007865, \ldots, 1142162\}$. Series $\{y_1(k)\}$, $\{y_2(k)\}$ and $\{y_3(k)\}$ are the echo time series of the CROW, CW and LFMU pulses,

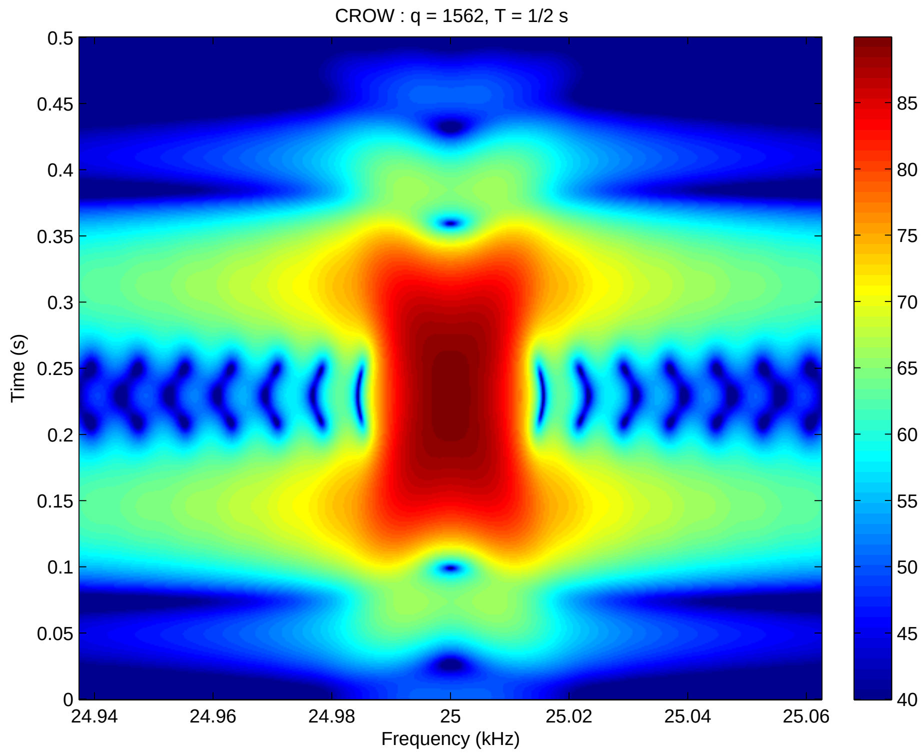

Figure 2. Spectrogram of transmitted CROW pulse, on a logarithmic scale.

respectively. The transmitted pulses were sampled at the same rate $F_s = 131\,072\,\mathrm{Hz}$ and stored in the corresponding time series $\{x_1(l)\}$, $\{x_2(l)\}$ and $\{x_3(l)\}$, respectively, over absolute times $t = lT_s$ where $l \in \{1, ..., L\}$ for $L = TF_s = 65536$. Each of the six time series $\{x_1(l)\}$, $\{x_2(l)\}$, $\{x_3(l)\}$, $\{y_1(k)\}$, $\{y_2(k)\}$ and $\{y_3(k)\}$ was processed with the discrete Hilbert transform to form a discrete analytic signal [4]. Subsequently, each series was forced to have a mean of zero by calculation and removal of the sample mean. Finally, the zero mean echo time series data $\{y_1(k)\}$, $\{y_2(k)\}$ and $\{y_3(k)\}$ were normalized to a variance (mean power) of unity. Circular white Gaussian noise was added to each normalized echo time series at Signal–to–Noise Ratios (SNRs) of -34, -36, -38, -40 and $-42\,\mathrm{dB}$, where the SNR was given simply by $\mathrm{SNR} = -10\log_{10}(2\sigma^2)$, with σ^2 being the variance of each of the independent real and imaginary components of the complex Gaussian noise.

For each realisation $\{n_j(k)\}$ of additive noise at a given SNR, for $j \in \{1, 2, 3\}$, noisy signals $y_j(k) + n_j(k)$ were formed and processed with a detection algorithm. The CW and LFMU signals were analyzed with a narrowband cross ambiguity detector, with detection statistic

$$\mathcal{A}_j = \max_{r,s} \left| \sum_{l=1}^{L} x_j^*(l) w_j(r+l) e^{-2\pi i s(l-1)/L} \right|, \quad j \in \{1, 2, 3\}, \tag{11}$$

where $x_j^*(l)$ is the conjugate of $x_j(l)$ for $l \in \{1, ..., L\}$ and where

$$w_j(k) = \begin{cases} n_j(k) & \text{noise only,} \\ y_j(k) + n_j(k) & \text{signal plus noise.} \end{cases} \tag{12}$$

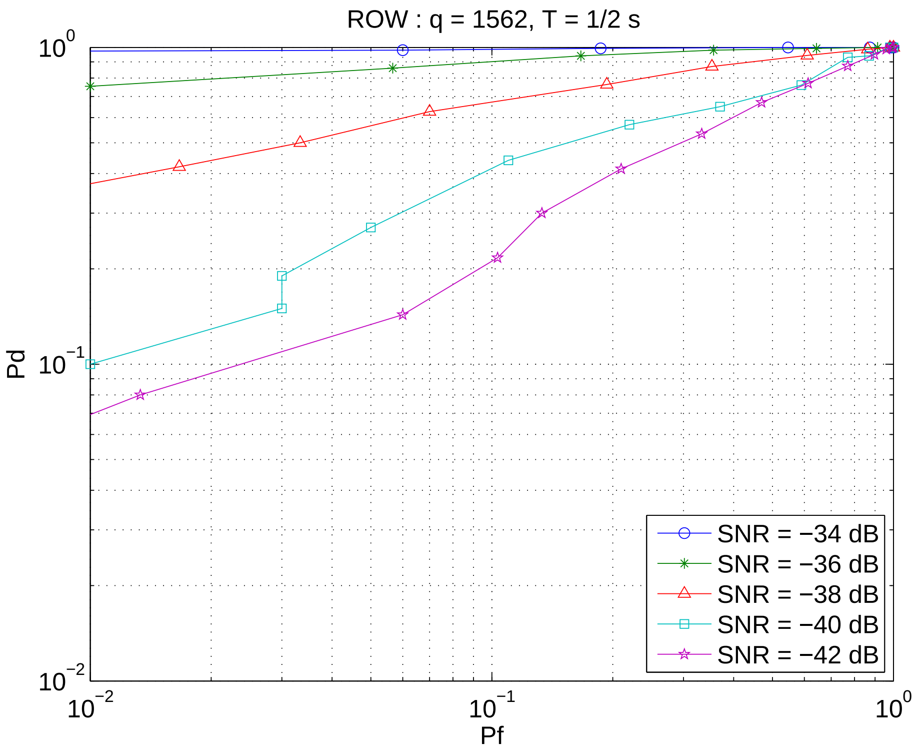

Figure 3. Empirical ROC curves for the ROW pulse.

Indexes r and s in (11) refer to a delay of $\tau = rT_s$ seconds and a Doppler shift of $\nu = sF_s/L$ Hertz.

The detector for the CROW signals uses a filter bank of scaled wavelets $\psi_m(t) = \psi\,(a^m t)$, where $a = 1 + (1/q)$ is the rational scaling factor and $m \in \mathbb{Z}$. Whereas the narrowband detector uses a discrete grid over delay and Doppler co–ordinates (indexed by integers r and s, respectively), the (wideband) CROW detector uses a discrete grid over delay and *scale* co–ordinates, where the index of the scale co-ordinate is m. Essentially, for a given m, that is, for a given filter function $\psi_m(t)$ in the bank of scaled filters $\{\psi_m(t)\}$, a correlation is formed of the received 'signal' $w_j(t)$ with a delayed version $\psi_m(t-\tau)$ of the filter $\psi_m(t)$. The output statistic is the maximum magnitude of this correlation over all discrete delay and scale co–ordinates.

Figures 3, 4 and 5 are plots of the empirical Receiver Operating Characteristic (ROC) curves for the three pulses studied in this paper. Each ROC curve is derived from several hundred independent realisations of the circular Gaussian noise process at each of the SNR values shown. For each realisation, the output of a detector was produced for the two cases of noise only and signal plus noise. This produced empirical estimates of the probability density functions (PDFs) of the detector, from which we estimated the probabilities of false alarm (P_f) and detection (P_d).

The superiority of the wavelet pulse is apparent. For a probability of false alarm of 10^{-2} and at an SNR of -38 dB, for example, the wavelet pulse (figure 3) has a probability of detection of about 0.4, compared to the value 0.1 for the CW pulse (figure 4), a four–fold improvement. Given the tactical requirement to detect targets as early as possible, this performance gain is significant. At the low SNR values used in this study, the LFMU pulse was a poor detector. Most of the curves for the LFMU pulse are close to the straight line from (P_f,P_d) co-ordinates $(10^0, 10^0)$ to $(10^{-2}, 10^{-2})$, this line being the theoretical noise–only limit.

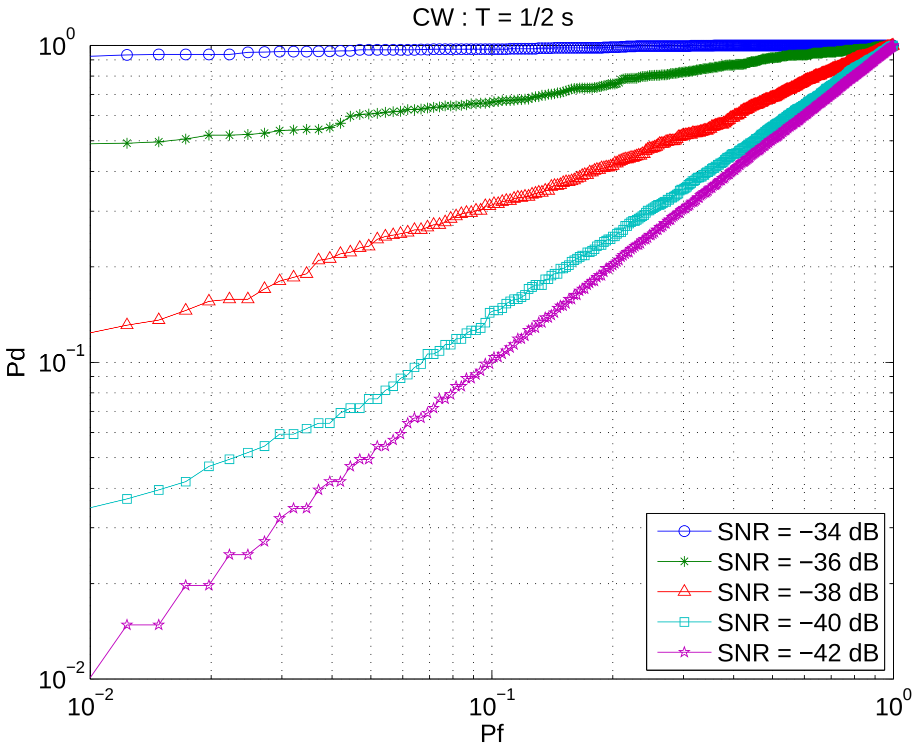

Figure 4. Empirical ROC curves for the CW pulse.

We can explain the performance benefit of the wavelet pulses with reference to the theory discussed in section 2. There, we mentioned the fact that the set of scaled and delayed copies $\{\psi_{+,kl}(t)\}$, $k, l \in \mathbb{Z}$, of the basic CROW $\psi_+(t)$ forms an orthonormal basis of the complex–valued Hilbert space $L^2(\mathbb{R})$. What this means in practice is that we can represent any received (complex–valued) time series $y(t)$ as a series over the set of basis functions $\{\psi_{+,kl}(t)\}$, $y(t) = \sum_{k,l} c_{kl}\psi_{+,kl}(t)$, say, where $\{c_{kl}\}$ is a set of wavelet coefficients to be determined. Determining the wavelet coefficients is analogous to the procedure of performing Fourier analysis with the Discrete Fourier Transform (DFT), where we find the coefficients in an expansion of $y(t)$ in terms of sine and cosine functions, these being another orthonormal basis of $L^2(\mathbb{R})$. The wavelet filter bank is an analogue of the DFT. By working with the dimensions of delay and scale, instead of the dimensions of phase and frequency of the Fourier domain, wavelets are better matched to the delay and scale pulse distortions occurring in shallow water.

5. CONCLUSIONS

The Rational Orthogonal Wavelet was recently demonstrated to show promise in a communications setting [3]. We have conducted preliminary investigations that indicate the applicability of ROW pulses to the detection of fast–moving targets in the presence of multipath Doppler spread, a deleterious phenomenon that is the bane of naval operations in shallow water. In the present work we have demonstrated the superior detection performance at low SNR of wavelet pulses, when compared against more traditional CW and LFM pulses. In future work, we aim to explore the potential of ROW pulses in the detection context further, looking to more rigorous simulations and at–sea trials. The ability to exploit the extra dimension of diversity afforded by

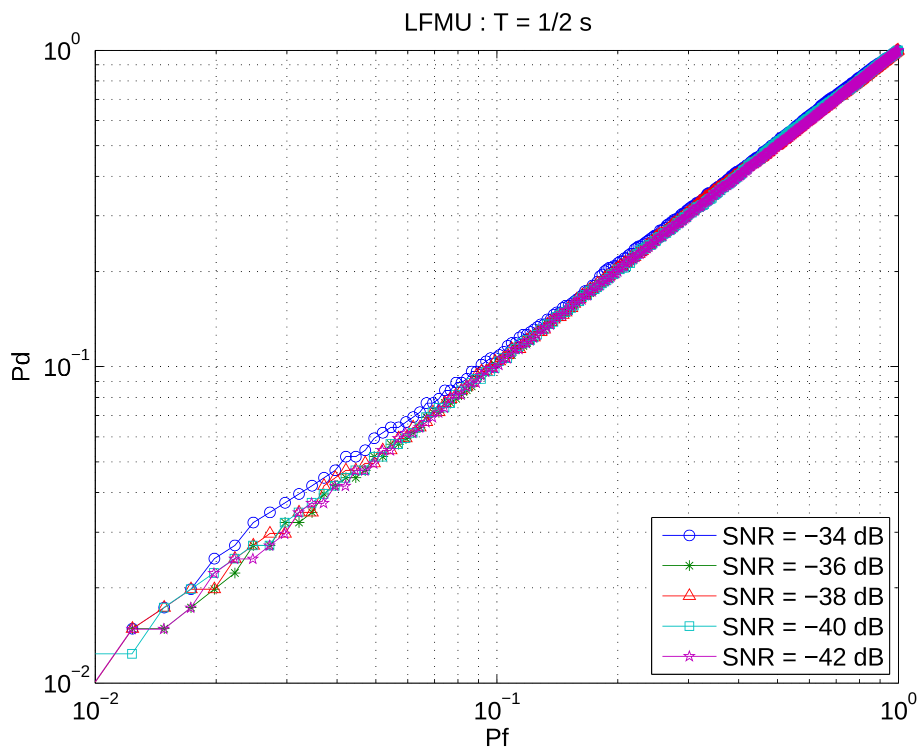

Figure 5. Empirical ROC curves for the LFMU pulse.

the set of dominant eigenpaths augurs well for the further application of the wavelet pulse in shallow water detection.

REFERENCES

[1] Wikipedia contributors, “4G”, *Wikipedia, The Free Encyclopedia*, April 1, 2007, 01:12 UTC, http://en.wikipedia.org/w/index.php?title=4G&oldid=119386686 (accessed April 11, 2007).

[2] G. Lawton, “What lies ahead for cellular technology?”, *Computer*, **38**, 14-17(2005).

[3] L. Yu and L.B. White, “Complex rational orthogonal wavelet and its application in communications”, *IEEE Signal Processing Letters* **13**, 477-480(2006).

[4] Wikipedia contributors, “Hilbert transform”, *Wikipedia, The Free Encyclopedia*, December 31, 2006, 05:43 UTC, http://en.wikipedia.org/w/index.php?title=Hilbert_transform&oldid=97487381 (accessed April 11, 2007).

[5] D.D. Ellis and D.M.F. Chapman, “A simple shallow water propagation model including shear wave effects”, *Journal of the Acoustical Society of America* **78**, 2087-2095(1985).

[6] R.E. Francois and G.R. Garrison, “Sound absorption based on ocean measurements: Part I:Pure water and magnesium sulfate contributions”, *Journal of the Acoustical Society of America*, **72**, 896-907(1982).

[7] F.B. Jensen and W.A. Kuperman, “Optimum frequency of propagation in shallow water environments”, *Journal of the Acoustical Society of America*, **73**, 813-819(1983).

[8] G.V. Frisk, *Ocean and seabed acoustics*, Prentice Hall, Englewood Cliffs, NJ, 1994.